

# Key Differences For Process-induced Uniaxial vs. Substrate-induced Biaxial Stressed Si and Ge Channel MOSFETs

S.E. Thompson, G. Sun, K. Wu, J. Lim, and T. Nishida  
University of Florida, PO Box 116130, Gainesville FL 3261

## Abstract

For both n and pMOSFETs, this paper confirms via controlled wafer bending experiments and physical modeling the superiority of uniaxial over biaxial stressed Si and Ge MOSFETs. For uniaxial stressed p-MOSFETs, valence band warping creates favorable in and out-of-plane conductivity effective masses resulting in significantly larger hole mobility enhancement at low strain and high vertical field. For process-induced uniaxial stressed n-MOSFETs, a significant performance advantage results from a smaller threshold voltage shift due to less bandgap narrowing and the gate also being strained.

## Introduction

The pioneering work on strained Si MOSFETs during the last 20 years has focused on tensile biaxial substrate stress. This was driven by the hope that biaxial stress could improve both n and p-MOSFETs simultaneously. Although this is true, it occurs only at low electric field and high stress [1,2]. Recently, uniaxial stress has become the preferred method to strain the Si lattice and has been implemented into several 90 nm logic technologies [3-6]. The goal of this paper is to confirm the differences for biaxial and uniaxial stress and explain for the first time the physical mechanism responsible.

## Strained Si Data

Nearly all the experimental data suggest that uniaxial stress has key advantages in both the mobility enhancement and threshold voltage shift. Summarizing the experimental data, uniaxial unlike biaxial stress has significant hole mobility enhancement at low stress and high vertical electric fields and an advantageously small nMOSFET threshold voltage shift. Since many process flow parameters are changed when fabricating strained MOSFETs, there is some uncertainty if strain alone is responsible for the above experimental data. To gain confidence in the above observations, four point longitudinal and transverse uniaxial and concentric ring biaxial wafer bending experiments are used as a quantitative check of the above observations. Wafer bending mechanical stress is calculated from local wafer curvature measured with a laser. For the biaxial wafer bending, material anisotropy is neglected even though silicon is orthotropic.

The mobility is extracted from changes in the linear drain current and shown in Fig. 1 for the six possible types of stresses. Transistors from a standard 90 nm technology [3-6] are used in the wafer bending measurements. In general, the wafer bending data support the above biaxial substrate and uniaxial process induced stress observations. Longitudinal uniaxial compressive stress is observed to cause much larger hole mobility enhancement at low and moderate stress on pMOSFETs. Furthermore, consistent

with the uniaxial process stress data, enhanced hole mobility is observed at both low and high vertical fields as shown in Fig. 2. Wafer bending uniaxial tensile stress also shows a small threshold voltage shift for nMOSFETs which will be presented in the next section.

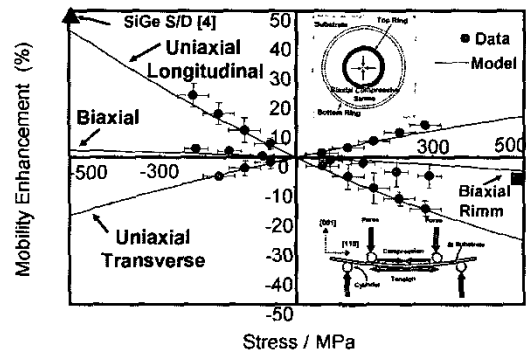


Figure 1: Enhanced mobility vs. stress induced via wafer bending: biaxial and longitudinal and transverse uniaxial stress.

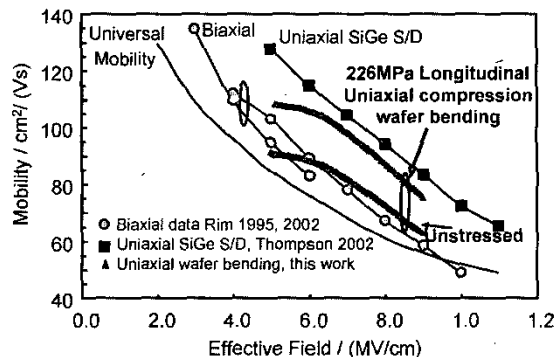


Figure 2: Strained Si hole mobility enhancement vs. vertical electric field (wafer bending, SiGe S/D, biaxial substrate stress).

## Physical Insight into the Experimental Data

With the wafer bending data supporting several advantages for uniaxial process stress, we next explore the physical mechanisms responsible. State-of-the-art transport modeling consists of full-band Monte Carlo simulations using non-local empirical pseudopotentials method to determine the strained Si band structure [2, 3]. However, at present the hole transport mechanisms and larger n-MOSFET threshold-voltage shift for biaxial stress are not understood and have yet to be modeled. To facilitate understanding the essential physics, we use a simpler formalism which consist of solving the 6x6 Luttinger-Kohn Hamiltonian to calculate the strain altered band structure, analytical scattering models, and deformation potential theory to calculate the band edge shift needed to determine the MOSFET threshold voltage shift. Band parameters from Ref. [7] are used in this work.

### A. Hole Mobility Enhancement at Low Stress

To quantify the mobility enhancement, changes in the conductivity effective mass and scattering are taken into account both of which depend on the strain-altered valence band. The calculated valence band constant energy surfaces and x-y contours in the MOSFET conduction plane are shown for the highest energy band in Fig. 3 for unstressed, longitudinal uniaxial compressive, and biaxial tensile stress. Several interesting differences are observed. First, for both biaxial and uniaxial stressed Si, the effective mass unlike for the unstressed case is approximately constant over the energy range of a few kT. The approximately constant effective mass results since strain removes the degeneracy and reduces the band-to-band coupling. Second, the valence band under uniaxial compressive stress not only causes a repopulation in k space along  $\langle 1-10 \rangle$  [3] but also significantly superior in-plane conductivity mass. In-plane effective masses in the x-y plane for transport along the  $\langle 110 \rangle$  channel direction are labeled and show  $\sim 40\%$  lighter effective mass for uniaxial stress. It is this superior in-plane mass for uniaxial stress that results in enhanced mobility at low strain.

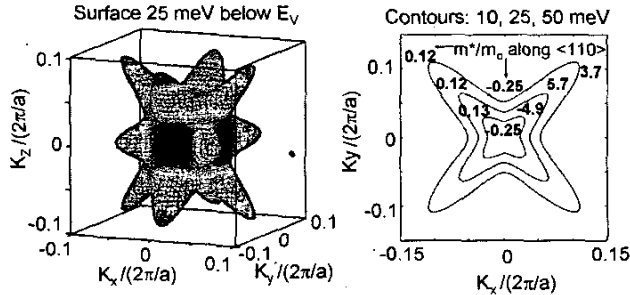


Figure 3(a): Unstressed Si band structure. Constant energy surface at 25meV below valence band and constant energy contours in x-y plane. Conductivity effective mass labeled in contour plot along  $\langle 110 \rangle$ .

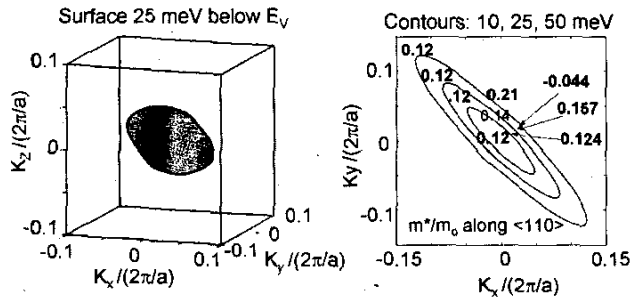


Figure 3(b): 1GPa longitudinal uniaxial compressive stress.

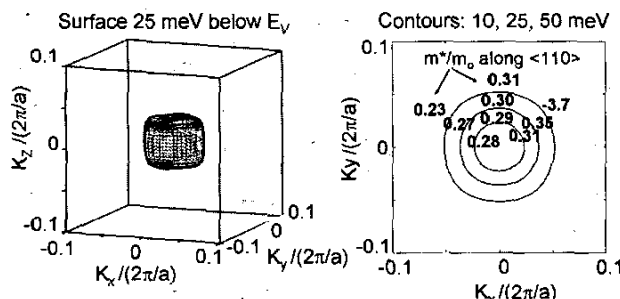


Figure 3(c): 1G biaxial tensile stressed Si band structure. Note the larger effective mass for biaxial stress.

Changes in scattering could also contribute to the hole mobility improvement but will be shown to be a small at the current ( $\sim 500\text{MPa}$ ) [4] and even larger ( $\sim 900\text{MPa}$ ) [6] uniaxial stress. Strain reduces the acoustic scattering rate via altering the light and heavy hole band density of states and/or by reducing interband optical phonon scattering through light to heavy hole band splitting. The change in intraband acoustic phonon scattering is proportional to  $(m_{\text{DOS}})^{3/2}$  which when estimated by treating the constant energy surfaces as ellipsoids  $(m_{\text{DOS}})^{3/2} = (m_l m_h^2)^{1/2}$  only changes a few percent at 500MPa of stress. Next, interband optical phonon scattering is estimated by considering that holes undergoing a scattering event must adjust energy by the light to heavy hole band splitting ( $\Delta E_s$ ). The band splitting reduces the post scattering density of allowable states which leads to the interband optical phonon scattering being proportional to

$$\sqrt{E - \Delta E_s + \hbar w_o} + e^{\hbar w_o / kT} \sqrt{E - \Delta E_s - \hbar w_o}$$

where  $\hbar w_o$  is the optical phonon energy ( $\sim 60\text{meV}$  in Si). The scattering rate only significantly decreases if the light to heavy hole band splitting is comparable to the optical phonon energy. Figure 4 shows the band splitting at  $k=0$  as a function of stress. Significant scattering reduction requires  $>1\text{GPa}$  of stress to split the band 60 meV which is consistent with the biaxial substrate hole mobility experimental data [1]. For biaxial stress since there is no mass improvement, the mobility enhancement only results from reduced scattering and thus requires  $\sim 25\text{-}30\%$  Ge ( $>1\text{GPa}$  stress) [1].

Since under strain, the effective mass is approximately constant and changes in the scattering small, a simple analytical model is sufficient to capture the essential physics and quantitatively and accurately match the hole mobility change vs. the six types of stress in Fig. 2. Taking into account only the light and heavy hole mass change and band repopulation ( $\sigma = q\tau^2 (p_{lh}/m_{lh} + p_{hh}/m_{hh})$ ) the calculated mobility vs. stress are the solid lines in Fig. 1 and shows good agreement with the experimental data. The in-plane mass at  $k=0$  is used where analytical expression exist since the numerical results in Fig. 3 suggest under strain the mass is relatively constant in the energy range of a few kT. Lastly, to gain confidence in the simpler 6x6 strain Hamiltonian band calculations, the calculated strained altered valence band structure is compared and shown in Fig. 5 to be similar to the numerically intensive empirical pseudopotentials [3] method.

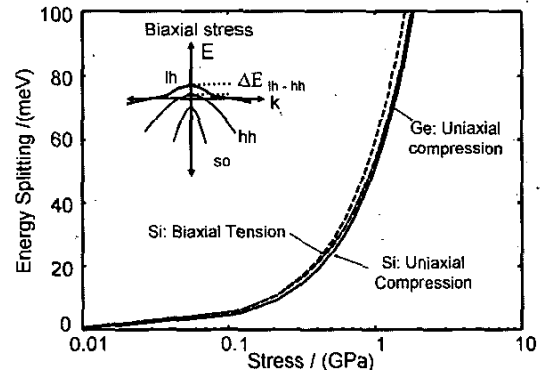


Figure 4: Light minus heavy hole band splitting for uniaxial and biaxial strained Si and Ge (not including 2D surface quantization). Similar energy splitting for uniaxial and biaxial stress.

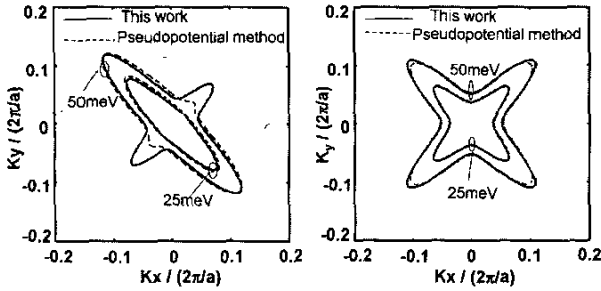


Figure 5: Valence band structure for 500MPa compressive stress. 6x6 strain Hamiltonian compared to the pseudopotentials[1] method.

### B. Hole Mobility vs. Vertical Field

Next we explain why the uniaxial hole mobility enhancement is present at high vertical electric field. In a MOSFET, the 2-dimensional surface confinement also shifts the light and heavy hole bands. Using the empirical pseudopotential method, Fischetti recently showed surface confinement cancels the biaxial stress light to heavy hole band splitting [2] causing the enhanced mobility to be lost at high vertical fields. In contrast, uniaxial hole mobility data suggest the splitting is not cancelled by surface confinement which is a major advantage for modern nanoscale MOSFETs which operate at >5 MV/cm oxide electric fields.

Since under strain as shown in Fig. 3, the hole effective mass is relatively constant in k space, an effective mass approximation for the out-of-plane direction and Schrödinger equation is used to calculate the light to heavy hole splitting due to 2D surface confinement (Fig. 6). The magnitude of the surface confinement splitting depends on the relative magnitude of the stress altered light and heavy hole out-of-plane effective masses. For uniaxial stress, the out-of-plane mass is calculated from the 6x6 Hamiltonian for Si and Ge in Fig. 7. Both Si and Ge show the interesting result that for uniaxial stress,  $m_{lh}^z > m_{hh}^z$  which causes the light to heavy hole band splitting to **increase** with surface confinement while for biaxial stress the previously reported  $m_{lh}^z < m_{hh}^z$  causes the band splitting to be reduced (“canceled” [2]) by surface confinement. Previously Fig. 4 shows similar uniaxial vs. biaxial stress induced splitting (without surface confinement). Including confinement and for 500 MPa of uniaxial or biaxial stress, Fig. 8 shows the band splitting vs. vertical electric field. The band splitting caused by surface confinement is additive for uniaxial but subtractive for biaxial stress which is consistent with the experimental hole mobility data. The value of this simple formulism is that it captures the essential physics and shows for the first time the physical origin of quantum confinement differences for uniaxial and biaxial stress.

In summary the experimental data and band calculations support uniaxial stress having an advantageous in and out-of-plane effective mass. Thus, the valence band warping under uniaxial and biaxial stress must look qualitatively as shown in Fig. 9.

### C. Strain Induced MOSFET Threshold Shift

Lastly, for biaxial tensile stressed nMOSFET, large strain induced threshold voltage shifts occur[8]. Since perform-

ance benchmarking needs to be done at constant off-state leakage, the threshold voltage shift must be corrected (typically accomplished by higher well doping) which increases ionized impurity scattering and has recently been shown to cause most of the enhanced electron mobility to be lost [9].

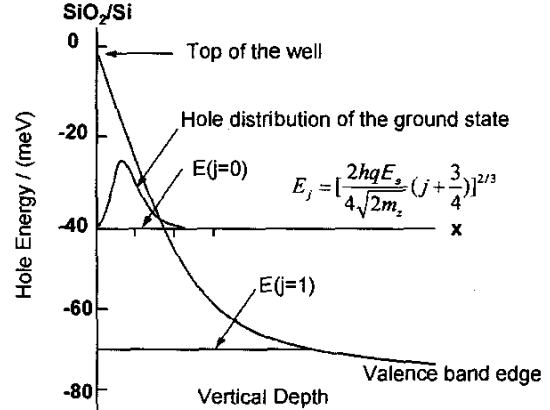


Figure 6: Hole energy level shift due to 2D quantization.

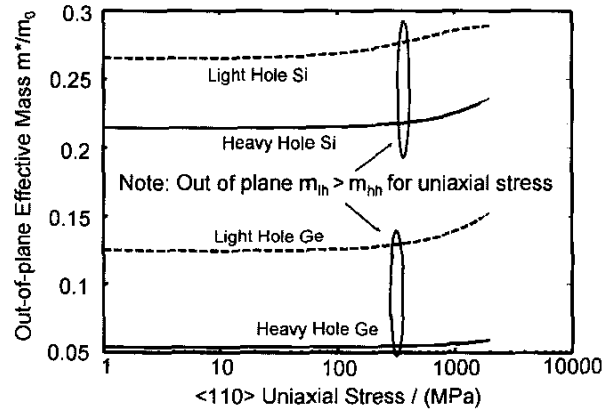


Figure 7: Strained Si and Ge MOSFET out of plane hole effective mass vs. uniaxial strain (note  $m_{lh}^z > m_{hh}^z$  for both strained Si and Ge).

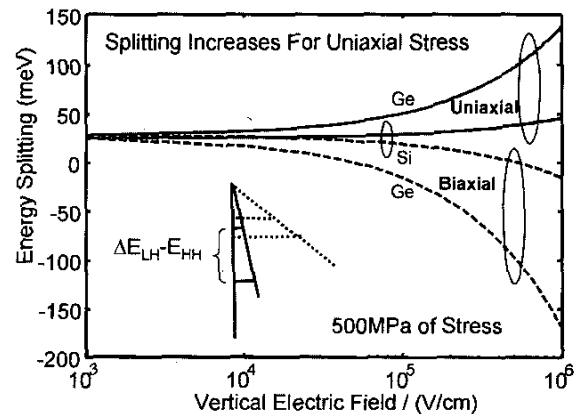


Figure 8: Light minus heavy hole band splitting in strained Si and Ge channel MOSFETs for 500MPa of stress vs. vertical electric field (splitting “additive” for uniaxial stress).

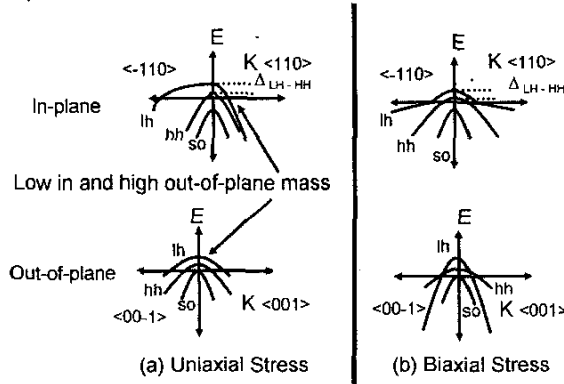


Figure 9: Simplified valence band E vs. k diagram for strained Si or Ge.

To quantify the strain induced nMOSFET threshold voltage shift, deformation potential theory is used to calculate electron affinity, bandgap narrowing, and density of states as a function of biaxial and uniaxial stress. The deformation parameters used in this work are listed in Table 1 [10]. With these quantities the threshold voltage shift is giving by

$$q\Delta V_{th}(\sigma) = \begin{cases} \Delta E_c(\sigma) + (m-1) \left[ \Delta E_g(\sigma) + kT \ln \frac{N_v(0)}{N_v(\sigma)} \right] & \text{biaxial} \\ (m-1) \left[ \Delta E_g(\sigma) + kT \ln \frac{N_v(0)}{N_v(\sigma)} \right] & \text{uniaxial} \end{cases}$$

where  $m$  is the body coefficient,  $E_c$  the conduction band edge,  $E_g$  the energy gap and  $N_v$  the valence band density of states. The larger threshold shift for biaxial stress results from two effects. First biaxial tensile stress causes larger Si channel bandgap narrowing as shown in Fig. 10. The larger bandgap narrowing results for several reasons one being a larger shift in the valence band edge for biaxial than uniaxial stress. This occurs since the light (vs. heavy) hole band shifts more and the valence band edge is set by the light hole band for biaxial tensile stress while being set by the heavy hole for uniaxial tensile stress (not to be confused with uniaxial compressive stress where the light hole band is the top band). Second, uniaxial process strain does not have a  $\Delta E_c$  term since the gate is also strained. The  $V_T$  shift is calculated using the above equations for two sets of deformation potentials and shown in Fig. 11. The two sets of deformation potentials are used to bracket the large uncertainty in this material property. The calculated threshold voltage shift is at least 4x larger for biaxial than uniaxial stress. The  $V_T$  shift is in agreement with uniaxial wafer bending and published biaxial strained Si on relaxed SiGe MOSFET experimental data included in Fig. 11.

### Conclusion

The results suggest that uniaxial stress will be the dominant type of stress adopted in logic technologies due to advantages observed for both n and pMOSFETs. When adding new technology options to extend Moore's Law, it is important to consider if the improvement is present with future device scaling. Since uniaxial stress hole mobility enhancement results from a mass instead of a scattering improvement, the enhanced hole mobility improvement will be present in a nanoscale ballistic transport limited MOSFET[11].

Table 1: Si Electron affinity and bandgap narrowing calculated as a function of strain. Lines 2 and 3 brackets uncertainty in  $\Xi_d$ .

Stress type	Deformation potential constants [eV]	$\Delta E_c(\sigma)$ [eV]	$\Delta E_g(\sigma)$ [eV]
[110] Uniaxial	$\Xi_d = 1.13$ $\Xi_u = 9.16$	$a = 2.46$ $b = -2.35$ $d = -5.08$	$-2.66\epsilon$ $-6.19\epsilon$
Biaxial (1)	$\Xi_d = 1.13$ $\Xi_u = 9.16$	$a = 2.46$ $b = -2.35$	$-5.67\epsilon$ $-17.01\epsilon$
Biaxial (2)	$\Xi_d = -10.7$ $\Xi_u = 10.5$	$a = -9.7$ $b = -2.33$	$-41.04\epsilon$ $-44.72\epsilon$

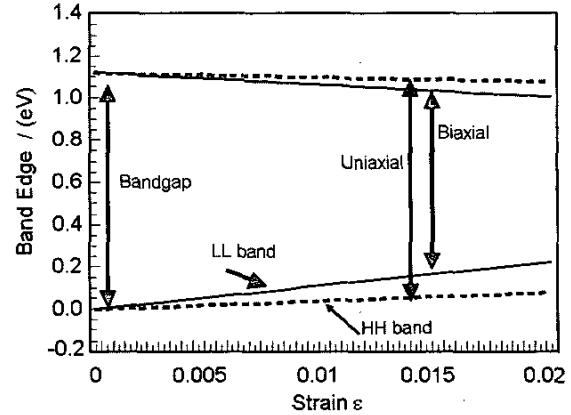


Figure 10: Using deformation potential theory, calculated Si conduction and valence band shift for uniaxial and biaxial stress.

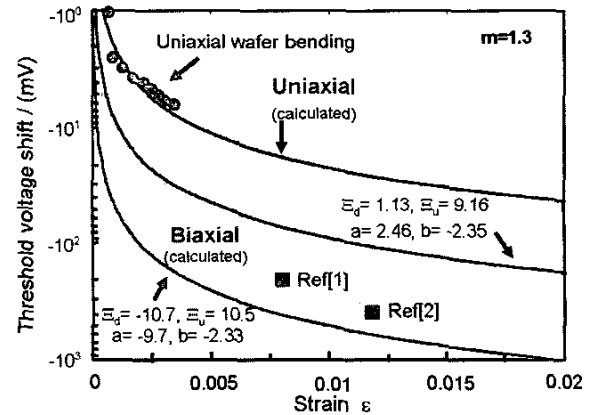


Figure 11: Calculated and measured threshold voltage shift for nMOSFETs under uniaxial and biaxial stress (>4x shift for biaxial stress).

### References

- [1] C.W. Leitz, et al., *J. Appl. Phys.* pp. 3745-51, 2002.
- [2] M.V. Fischetti et al., *J. Appl. Phys.* pp. 1079-95, 2003.
- [3] M. Giles et al., *VLSI Technology*, ses. 12.2, 2004.
- [4] S. Thompson et al., *Elec. Device Lett.*, pp. 191-3, 2004.
- [5] V. Chan et al., *IEDM*, pp. 77-80, 2003.
- [6] P.R. Chidambaram et al., *VLSI Technology*, ses. 6.1, 2004.
- [7] P. Lawaetz, *Phys. Rev. B* 4, pp. 3460-3467, 1971.
- [8] J. Goo et al., *Elec. Device Lett.*, pp. 568-70, 2003.
- [9] J. G. Fossum et al., *Trans. Elect. Dev.* pp. 1042-9, 2003.
- [10] J.Lim, S.E.Thompson, J.G. Fossum accepted *EDL*, 2004.
- [11] M. S. Lundstrom, *Trans. Elec. Dev. Lett.* p361-3 1997.